Investigation of the Gas-Liquid Flow in an Agitated Vessel Equipped with an ASI Impeller by Using Tomography Method

Khalili, Fariba; Jafari Nasr, Mohammad Reza*[+•]

Department of Chemical Engineering, Science and Research Branch, Islamic Azad University, Tehran, I.R. IRAN

Ein-Mozaffari, Farhad

Department of Chemical Engineering, Ryerson University, 350 Victoria Street, Toronto, M5B 2K3, CANADA

Soltaniye, Mohammad

Department of Chemical Engineering, Science and Research Branch, Islamic Azad University, Tehran, I.R. IRAN

ABSTRACT: *In this study, the hydrodynamics of the gas dispersion in an aerated vessel equipped with a newly designed impeller (ASI impeller), a combination of the pitched blade turbine and the Scaba impeller was investigated. The performance of the ASI impeller was compared with the performances of the pitched blade turbine and the Rushton impeller. The non-invasive Electrical Resistance Tomography (ERT) technique was used to assess the gas dispersion inside the mixing vessel. The effects of the volumetric gas flow, and impeller type and speed were investigated on power drawn, gas holdup, and mixing time. An analysis of the experimental data indicated that the ASI impeller exhibited a minimal effect of the gassing on the power drawn compared to the pitch blade and the Rushton turbine. Measured data on gassed power consumption indicated that the ASI impeller was about 45% more efficient than the Rushton turbine and 20% more than the downward PBT under the general operating conditions in bioreactors for gas flow rate about 1 vvm. Also, this impeller showed a higher amount of gas hold up and lower mixing time compared to the two other studied impellers. A dimensionless correlation for the relative power consumption as a function of flow number and Froud number was developed for the aerated agitated tank. Also, a dimensionless correlation was introduced to compute the overall gas hold up as a function of specific power consumption and superficial gas velocity for the gas-liquid agitated system. Overall conclusion from this study demonstrated that the axial-radial ASI impeller is a good energy-efficient impeller for the aeration system and bioreactors based on the results from the investigation of the data in terms of the power consumption, gas holdup, and mixing time.*

KEYWORDS: *Electrical resistance tomography; Mixing time; Power consumption; Gas holdup; ASI impeller.*

***** *To whom correspondence should be addressed.*

+ E-mail: drnasr50@yahoo.ca

1021-9986/2020/4/321-338 18/$/6.08

INTRODUCTION

Effective contact between the liquid phase and the gas phase is important in many industrial processes for providing mass or heat transfer or producing a chemical reaction. There are some methods that provide effective contact between the gas and liquid phases. Packed columns trickle bed reactors and thin-film reactors are some typical processes in which the liquid phase flows as a thin film against the gas phase. In spray columns and venturi scrubbers, the liquid is dispersed as fine particles into the gas phase. In stirred tanks and bubble columns, gas is dispersed as bubbles into the liquid phase. Each of these contact methods has its applications and benefits. Bubble columns and gas-lift recirculating columns are cheap, and provide medium mass transfer performance. Sprays produce low liquid holdup, and contact time in the static mixers is short.

Gas–liquid mixing in stirred tanks is the dominant process in the chemical industry where high gas-liquid mass transfer levels are required and have been widely implemented for biological applications; they offer good performance because of their flexibility in mass and heat transfer. In addition to providing a good degree of homogeneity in the shortest time, they also accommodate a large variety of fluid viscosities and a wide range of operating conditions. *(Paul et al.,* 2004*; Hashemi et al.,* 2016*; Kadic* and *Heindel,* 2010*; zhu et al.,* 2009*).*

Pharmaceutical production, metallurgical processing, polymerization, petrochemicals manufacturing such as chlorination and hydrogenation (*Moucha et al.,* 2003*; Fujasova et al.,* 2007) and various fermentation systems such as mycelia aerobic cultures *(Kadic* and *Heindel.,* 2010*)* are some of the processes, which occur in gas- liquid stirred reactors.

An essential parameter for the design of all gas-liquid reactors is the gas holdup. The gas holdup is important for several reasons. The residence time of gas in the liquid, bubble size, available surface area for mass transfer, and accordingly the total design volume of the reactor have been controlled by the amount of gas holdup *(Vlaev et al.,* 2002*; Khare* and *Niranjan,* 2002*).* Because of its significant effect on the efficiency of gas–liquid contact, careful measurement of the local gas holdup and its changes with operational conditions are essential in aerated mixing systems. (*Hashmi et al.,* 2016*; Khare* and *Niranjan,* 2002). In stirred tank reactors, gas holdup is impressed with vessel and impeller design, steering velocity and power drawn, gas flow rate, rheology and physical properties of fluids. *(Khare* and *Niranjan,* 2002). Different techniques have been used by researchers to measure the local and global gas holdup *(Boyer et al.,* 2002*).* Radar probe, conductance probe (*Vlaev et al.,* 2002*),* Particle image velocimetry (PIV measurements) *(Montante* and *Paglianti,* 2015*; Zhu et al.,* 2009*)* and visual inspection level *(Moucha et al.,* 2003*; Bouaifi et al.,* 2001*; Mc Farlene et al.,* 1995*)* are the methods which have been widely used by researchers. The non-intrusive and non-invasive Electrical Resistant Tomography (ERT) technique is an attractive method, which has been used efficiently to measure two-phase flow parameters *(Wang et al.,* 2000*; Dong et al.,* 2003*; Montante* and *Paglianti,* 2015*; Hashemi et al.,* 2016*).*

Mixing time is also another important key with which to study the performance and hydrodynamics of stirred tank reactors. This parameter is comparable to the required time for estimating the controlling mechanism in a mass transfer process or a reaction *(Ascanio, 2015).* Generally, in stirred tank reactors, the necessary time for attaining a specific degree of homogeneity for the inserted tracer is defined as the mixing time (*Harnby et al., 1997*). Technically, there is a difference between the definition of bulk mixing time and local mixing time. The former is considered as the required time for achieving the uniform distribution in all points of vessel, and the latter is defined as how fast a material is distributed in a special zone of a tank. *(Ascanio, 2015).*

It should be noted that the mixing time in gassed conditions is different where aeration participates in the mixing especially at low impeller speed *(Gabelle et al., 2011; Taleshi et al 2016)*. Some researchers tried to get useful correlations of mixing time from experimental measurement, but it has been proven that they are not valid in other condition and other systems *(zhang et al., 2009)*. Different techniques, which are classified as direct or indirect measurement methods (e.g. conductivity measurement and pH method, thermography, Planar Laser-Induced Florescence (PLIF), electrical resistance tomography and Colorimetric method), have been utilized by some researchers for investigating the mixing time *(Ascanio,* 2015*).*

Power consumption is another key parameter with regard to industrial operating costs and mixing and

circulation times (*Gabelle et al.*, 2011). In an agitated system, the requisite specific power input for the complete dispersion of gas into a liquid phase at a specific gas flow rate is a function of the design of the impeller and system. In fact, power consumption can be regarded as an indicator of the efficiency of impellers in stirred gas dispersion systems (*McFarlen et al.*, 1995). In the literature surrounding a gas dispersion system, relative power draw (P_g/P_{ug}) is used as a criterion for process, which is defined as the power consumption reduction caused by the gas injection (*Michel* and *Miller*, 1962*; Tatterson* and *Kyser*, 1991; *Paul et al*., 2004; *Gabelle et al.*, 2011). Indeed, the lowest value of specific power input coupled with a high relative power uptake, can be one of the impeller design goals. In a stirred gas dispersion system, the power consumption is a function of the gas flow rate and the hydrodynamics of phases (*McFarlen et al*., 1995). Practical methods for determining the power drawn are based on measurements of the required torque for the system. There are many methods and devices for measuring the reaction torque; in all of them, care should be taken to avoid any frictional torque loads applied by bearings (*Paul et al*., 2004).

Research has shown that the efficiency of the agitated system is affected by the created flow pattern, which depends on the shape of the impeller. There are many requests from the industry for a more effectively designed mixing apparatus and reformation in the design of available impellers. The best type of mixer should be selected according to the goals of the mixing. One of the duties of the impeller in two- phase systems is to increase the intermediate surface area between adjacent phases for better heat or mass transfer (*McFarlen et al.*, 1995). Sparging of gas into the mixed liquid, provides more effective contact between phases (*Khare* and *Niranjan*, 2002).

An impeller that can preserve the gassed power level at approximately the same level as the un-gassed power level will give more stable operational conditions and can be considered as a suitable impeller in stirred gassed systems. For two-phase gas-liquid agitated systems, the introduced types of impeller with radial flow are hollow-blade impellers as the Scaba SRGT, Chemineer CD6 and BT6 and Lightning R130. Lightnin A345, A340 and the Prochem Maxflow are some types of wide-blade hydrofoils with axial-flow regime *(Paul et al.*, 2004).

The Rushton turbine is a radial mixer that has been widely used in two- phase gas-liquid systems and three phase gas-liquid-solid systems (*Khare and Niranjan*, 2002). However, this radial flow disc turbine has a number of disadvantages such as: poor top-to-bottom mixing, a significant fall of power consumption in the gassed condition, relatively high un-aerated power numbers, non-uniform distribution of energy dissipation rates, great energy loss in the impeller zone which can be destructive in fermentation and lead to stagnant zones in the outer reactor region (*Kadic* and *Heindel.*, 2010).

In spite of the improved performance of some types of axial-flow impellers relative to radial-flow impellers, the instabilities of power and torque, and non-uniformed stream lines especially in downward axial impellers in an aerated system have created increased requests to improve the design of these impellers in order to increase the efficiency of mixing.

Some studies show that for gas dispersion mixing systems the efficiency of impellers, which is defined as the ability to create maximum mass transfer coefficient besides the minimum power drawn, for a radial-axial impeller is more than that for a radial impeller or axial impeller configuration *(Mc Farlene et al.*, 1995).

Recently *Pakzad et al.* (2013) introduced the ASI impeller as a new axial-radial configuration impeller whose design is a combination of the pitched blade turbine as an axial impeller and the Scaba as a radial impeller. They studied the performance of this impeller in a non-Newtonian single phase system, and used it as a central impeller in a coaxial mixing system.

Therefore, the main objective of this study was to evaluate the performance of the ASI impeller in gas dispersion in a Newtonian fluid. In this study, Electrical Resistance Tomography (ERT) was utilized to characterize the hydrodynamics of the ASI impeller in a gas-liquid system in an agitated tank furnished with four baffles and a gas sparger. The influence of the gas flow rate and impeller speed was investigated with regard to mixing time, power up-take and gas holdup. The results are compared with those of both the Rushton turbine and downward Pitched Blade Turbine (PBT).

EXPEIRMENTAL SECTION

Experimental set-up

Experiments were conducted in a laboratory scale stirred tank that consisted of a flat-bottomed cylindrical vessel with a diameter (T) of 400 mm, and a height of 600 mm,

which was filled with water to a height of $H=T$. To avoid the formation of a vortex, the tank was equipped with four baffles of the same size, with a width of 33 mm (around 0.1T), and thickness of 5 mm, with a distance of 3mm (around T/50) from the inner surface of the vessels. A schematic diagram of our system is displayed in Fig. 1a.

Three types of impellers were used for this study. The main impeller- whose performance was studied-was the radial-axial ASI impeller *(Pakzad et al., 2013).* This impeller includes four blades angled at 45^0 which were attached to four curved blades with an inner diameter of 35 mm (referred to Fig. 1b). The distance between the impeller and the bottom of vessel was fixed on T/3.

Two other mixers compared to the ASI impeller were a six-bladed Rushton disk, and 4-blade 45^0 pitched down flow turbine, fabricated from PolyVinyl Chloride (PVC) with a thickness of 2 mm and a diameter equal to the ASI impeller.

The tank was furnished with top-entering shaft. The rotational speed of the Impeller was set by use of a variable frequency drive (Ac Technology Corporation). The impeller speed was changed from 10 rpm to 150 rpm. To check the rotational speed of the impellers, a tachometer (VWR, Germany) was used. A rotary–torque transducer with an encoder disc (Staiger Mohilo, Germany) was used for measuring the amount of torque.

A star-shaped sparger was used for air dispersion. Each branch of the sparger had a tube consisting of five holes, each 12 mm from the other and a diameter of 1mm. Each tube had a length of 6 cm, with an external diameter of 1.5 cm, made of PolyVinyl Chloride (PVC) with a thickness of 2 mm. The angle between the branches was 60^0. These six branches were connected to each other by a central hub. The outer diameter of the hub was 35 mm and was connected to the gas system. Sparger distance from the bottom of the vessel was 45 mm (around T/6). The flow rate of the Inlet gas was controlled and measured by a rotameter. The inlet gas flow rate was changed from 0.0000 m^3/s to 0.0008 m^3/s.

Tomography system.

An industrial tomography system (ITS, Manchester, UK, P2+V 7.0-2011) was used in this study for flow visualization. A typical electrical resistance tomography system (ERT) can determine the distribution of conductivity inside a vessel, by measuring the current or voltage difference between electrodes, which have equal distance from each other. The ERT system is composed of three parts; the first one is electrodes as the heart of system; the second one is a Data Acquisition System (DAS) which is located in a portable device and carries out signal measurement, demodulation, filtration, controlling and shearing the current source and voltage measurement. The third part is a computer with image reconstruction software *(Hashemi et al.,* 2016*; Pakzad et al.,* 2013*).*

As shown in Fig. 1a, six tomography sensor planes, each containing 16 stainless steel electrodes, were positioned around the vessels. These planes numbered from top to bottom and the lowest one was below the sparger with a distance of 10 cm from the bottom of the vessel. The distance between each plane was 4.5 cm and in each plane the distance between electrodes was 8 cm; they were located at equal distances around the tank. The height, width and thickness of each rectangular electrode was 2, 3, and 0.1 cm, respectively. The electrodes were connected to a Data Acquisition System (DAS) in order to measure the conductivity data. The set-up was equipped with a PC attached by a USB 2.0 cable.

In general, there are four major strategies for measuring voltage in a tomography system; adjacent strategy, opposite strategy, diagonal strategy and conducting boundary strategy. The first one is used in this study due to its fast reconstruction of images and less hardware being needed. This strategy injects a current by a pair of adjacent electrodes at one time, and the voltage difference is measured by the remaining pair of electrodes. The image reconstruction algorithm employed in this study was the linear back projection algorithm, which was used to obtain the 2D conductivity image for each plane from the voltage measurements.

Experimental material and procedure

The tank was filled with water up to 0.05 m^3 and air was injected at the bottom of the impeller by the sparger. For all experiments the temperature was kept constant around 22 ± 1 ^oC. For each experimental condition, power consumption was measured by using a rotary torque sensor installed on the shaft. The friction torque ($M_{friction}$) was measured when the vessel was empty, then the measured friction torque at any rotational speed was subtracted from the measured torque ($M_{display}$) to consider the effect of friction. The power consumption (P) for each operating

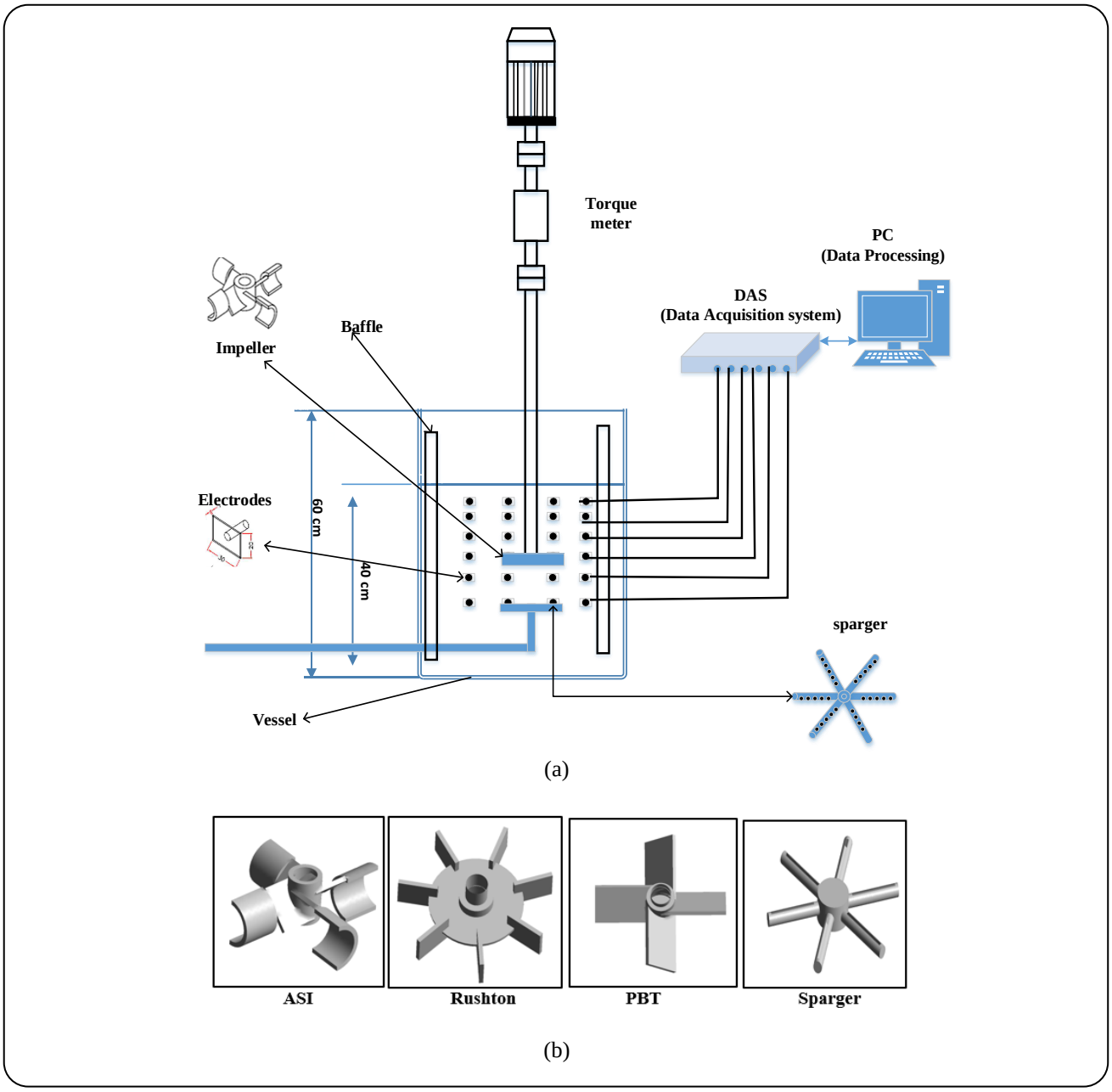

Fig. 1: (a) Experimental set up. (b) Impellers and gas sparger utilized in this study.

condition was then calculated by using the corrected torque (M) and the impeller speed *(Pakzad et al., 2008).*

To measure the gas holdup, the conductivity of the solution was monitored as a function of time for each gas flow rate (Q_g) and rotational speed (N), by using the ERT system. In order to eliminate the effect of the impeller and other components inside the tank, calibration of the ERT were performed before each measurement. In this case the reference states were measured as the impeller turned at the desired rate without gas. The average of 50 frames was utilized as reference frames to increase measurement accuracy.

In the aerated condition, the dispersion of gas reduces the conductivity of the solution. By measuring the average conductivity of all planes in the gassed condition and un-gassed condition, gas holdup can be determined by using Maxwell's equation for a two- phase gas-liquid system *(Manual ITS):*

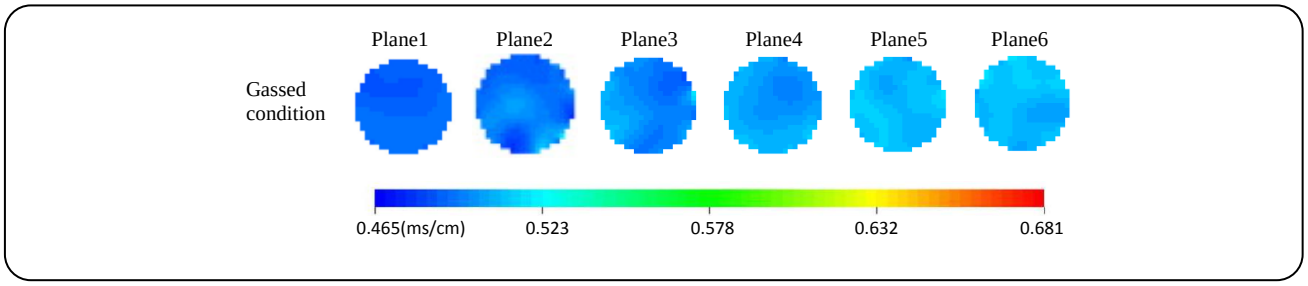

Fig. 2: Tomography images obtained for an aerated system equipped with the ASI impeller at Q_g = 0.0003 m^3/s and N = 80 rpm.

$$\varepsilon_g = \frac{2\sigma_1 + \sigma_2 2\sigma_{mc} - \frac{\sigma_{mc}\sigma_2}{\sigma_1}}{\sigma_{mc}\frac{\sigma_2}{\sigma_1}\sigma_{mc} + 2(\sigma_1 - \sigma_2)} \quad (1)$$

ε_g is the volume fraction of the dispersed material, σ_1 is the conductivity of the continuous phase, σ_2 is the conductivity of the dispersed phase and σ_{mc} is the measured local value of mixture conductivity. Since air is non-conductive, the Maxwell equation can be simplified for air-liquid system:

$$\varepsilon_g = \frac{2\sigma_1 - 2\sigma_{mc}}{2\sigma_1 + \sigma_{mc}} \quad (2)$$

In Fig. 2, tomogram images obtained from the ERT system were shown for the aerated conditions of the agitated system equipped with the ASI impeller at Q_g = 0.0003 m^3/s and N = 80 rpm. Each two- dimensional tomogram image was made by using 316 pixels. In this figure, light blue shows areas of higher conductivity with a smaller percentage of air bubbles, while the dark blue depicts areas with lower conductivity (which means the higher gas percentage). As can be seen from Fig. 2, a higher gas holdup was observed at Plane 6 (above the sparger) with darker blue image, and the lower gas holdup related to the Plane 1 near the liquid surface at the top of the tank.

Fig. 3 exhibits the conductivity changes of the solution as a function of time for Plane 1 to Plane 6 when water agitated by the ASI impeller at N = 80 rpm, and air was injected into the system at t = 10 s with a gas flow rate of 0.0003m^3/s. As this figure shows, before the gassing condition the conductivity of the six planes was about 0.537 ms/cm. By sparging the air at t = 10 s, the conductivity of all planes decreased. This figure shows that during the steady state of the aeration condition, the average value of conductivity for Plane 1 was about 0.429 ms/cm which is higher than other planes, and the lower conductivity (about 0.481 ms/cm) relates to Planes 6 and 5. These observations show that the gas holdup was lower at the upper part of the fluid in the tank and higher around the impeller and above the sparger.

To measure the mixing time by the ERT method, a solution of a more conductive 10% saline solution (5 mL) was injected with a syringe at the top of Plane 1 about 10 cm below the liquid surface, between the shaft and the inner surface of the tank. Due to the rotation of the impeller, this injected solution dispersed in all of fluid as a function of time. The changes in the conductivity of the solution were monitored as a function of time by ERT. By definition, the mixing time is the time between the injection of the brine solution and the time it takes the average fluid conductivity of six plane to reach 0.95% of conductivity value at all points in the tank in the steady-state condition. As can be seen from Fig. 4, after the injection of the brine at Q_g= 0.0005 m^3/s and N = 80 rpm for the ASI impeller, the conductivity of the solution suddenly increased from an average value around 0.36 ms/cm up to 0.65 ms/cm for Plane 1. After 5.8 s, the solution reached the 0.95% homogeneous distribution of brine.

The tomogram images that show the generated flow pattern inside the vessel at Q_g = 0.0005 m^3/s and N = 80 rpm for the ASI impeller are displayed in Fig. 5. The conductivity values are represented by different colored regions from rich blue for non-conductive (gassed phase) to the higher conductivity regions (red color).

Fig. 5, before the injection of saline solution, the tomogram images of the six planes have a blue color related to the low conductivity value because of the aerated condition. Injection of the brine created a high conductivity region with red color at the top of the tank

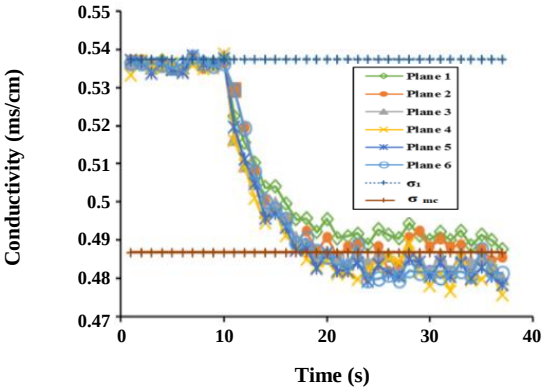

Fig. 3: Conductivity changes of the aerated water inside the aerated tank equipped by the ASI impeller at Q_g = 0.0003 m^3/s and N = 80 rpm.

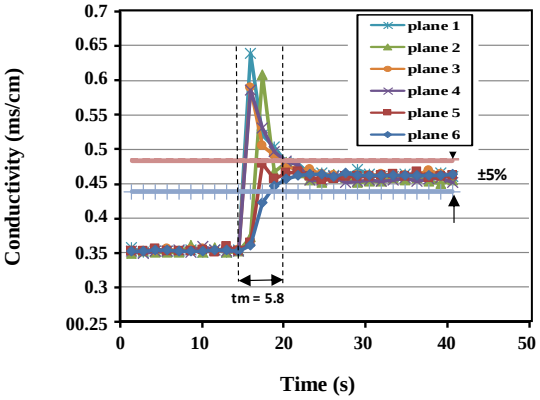

Fig. 4: Tomography images showing the dispersion of the tracer in the agitated water-air system furnished with the ASI impeller at Q_g = 0.0005 m^3/s and N = 80 rpm (Plane 1:z = 350 mm, Plane 2: z = 300 mm, Plane 3: z =250 mm, Plane 4: z = 200 mm, Plane 5: z =150 mm, and Plane 6: z =100 mm).

especially in the upper plane (plane 1 and plane 2). The downward movement of brine in the tank- due to the rotation of impeller- caused the conductivity of the planes to change over time and after 5.8s the brine was distributed in all parts of the tank. A homogenous green color of tomogram images can be seen for all six planes after this time. The small blue color at the bottom of the tank indicates the inlet gas zone in the gas injection region.

The dimensionless numbers (Power number (N_P), Reynolds number (Re), Flow number (Fl) and Froud number (Fr)), were calculated by using the following equations:

$$N_p = \frac{P}{\rho N^3 D^5} \quad (3)$$

$$Re = \frac{\rho N D^5}{\eta} \quad (4)$$

$$Fl = \frac{Q_g}{N D^3} \quad (5)$$

$$Fr = \frac{N^2 D}{g} \quad (6)$$

Where,P_{tot},ρ, N , D, η, and Q_g represent the total power consumption, density of the fluid, the impeller rotational speed, impeller diameter, fluid viscosity, and volumetric gas flow rate.

The measurements of power consumption, mixing time and gas holdup, were carried out at different rotational speeds of the impeller (N) and volumetric gas flow rates (Q_g) for all three mixers, under the same operating conditions. The experimental conditions for this study are summarized in Table 1.

Each experiment was done three times and the standard deviation was calculated by using the following equation:

$$SD = \sqrt{\frac{1}{n}\sum_{i=1}^{n}\left(Xi - \bar{X}\right)^2} \quad (7)$$

where n is the number of measurements, X is the variable and $\bar{X}$ is the mean value of variable.

RESULTS AND DISCUSSION

In order to study the hydrodynamic performance of the newly designed ASI impeller in an agitated system under aeration for Newtonian fluids, power consumption, gas holdup and mixing time were determined as a function of impeller speed and gas flow rate, and the experimental results were compared to those for the Rushton impeller and PBT.

Power consumption

For most impellers, because of the presence of cavities in the rear part of the blades, the power consumption under the gassed conditions is lower than that under the ungassed conditions (*Gabelle et al., 2011; McFarlane et al., 1995; Xie et al., 2014; Fujisova et al., 2007*). The effect of gas dispersion on power consumption in stirred tanks is assessed using the relative power consumption (P_g/P_{ug}) vs. the gas flow number. In order to investigate the hydrodynamic performance of different impellers in this

Table 1: Operating conditions in this study.

Description	Range and Type
Impeller types	ASI, Rushton turbine, 45^0 downward pitched blade.
Impeller speed	0 to 150 (rpm)
Gas flow rate	0.0000-0.0008 (m^3/s)

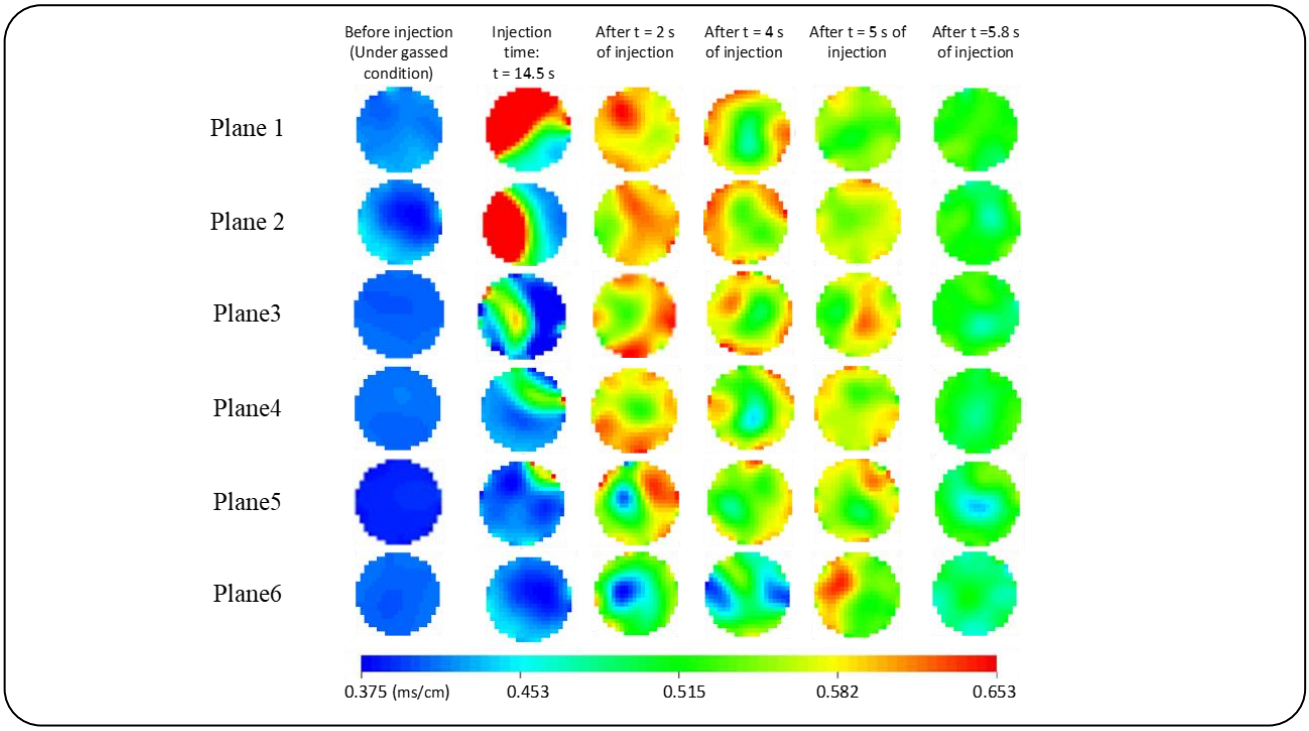

Fig. 5: Conductivity changes as a function of time after the injection of the tracer for the aerated system equipped with the ASI impeller at Q_g = 0.0005 m^3/s and N = 80 rpm.

study, a plot of relative power consumption as a function of the gas flow number for the ASI impeller, Rushton, and PBT was generated and is depicted in Fig. 6.

Fig. 6a shows the relative power consumption curves for the Rushton turbine at three different impeller speeds (N = 80 rpm, N = 110 rpm, N=140 rpm). As can be seen from this figure, with increasing the flow number, the power drawn decreased at all three impeller speeds. This figure also shows that P_g/P_{ug} decreased with increasing the rotational speed of the impeller at each flow number. Previous researchers have reported the same behavior for the influence of the flow number and impeller speed on the relative power consumption for the Rushton impeller in the aerated systems (*Paul et al.* 2004*; Paglianti et al.* 2001*; McFarlane* and *Nienow* 1996*; Woziwodzki* and *Broniarz* 2014).

As can be seen from Fig. 6a, the maximum reduction of relative power consumption were 30%, 32% and 35% at N = 80 rpm, N = 110 rpm and N=140 rpm, respectively under the conditions of $0.035 \leq Fr \leq 0.120$ and $Fl \leq 0.08$.

In aerated mixing tanks, gas bubbles tend to accumulate in low- pressure zones behind the impeller blades and form cavities that can reduce the power drawn for flat- blade disk turbines (*Paul et al., 2004*). *Nienow et al.* (1977) developed a relationship to estimate the relative power consumption of a single Rushton turbine. Based on this equation, increasing the flow number or impeller speed reduces the relative power consumption for the Rushton impeller (*Paul et al.*, 2004*; Woziwodzki* and *Broniarz*, 2014) and this is in accordance with the results in Fig. 6a.

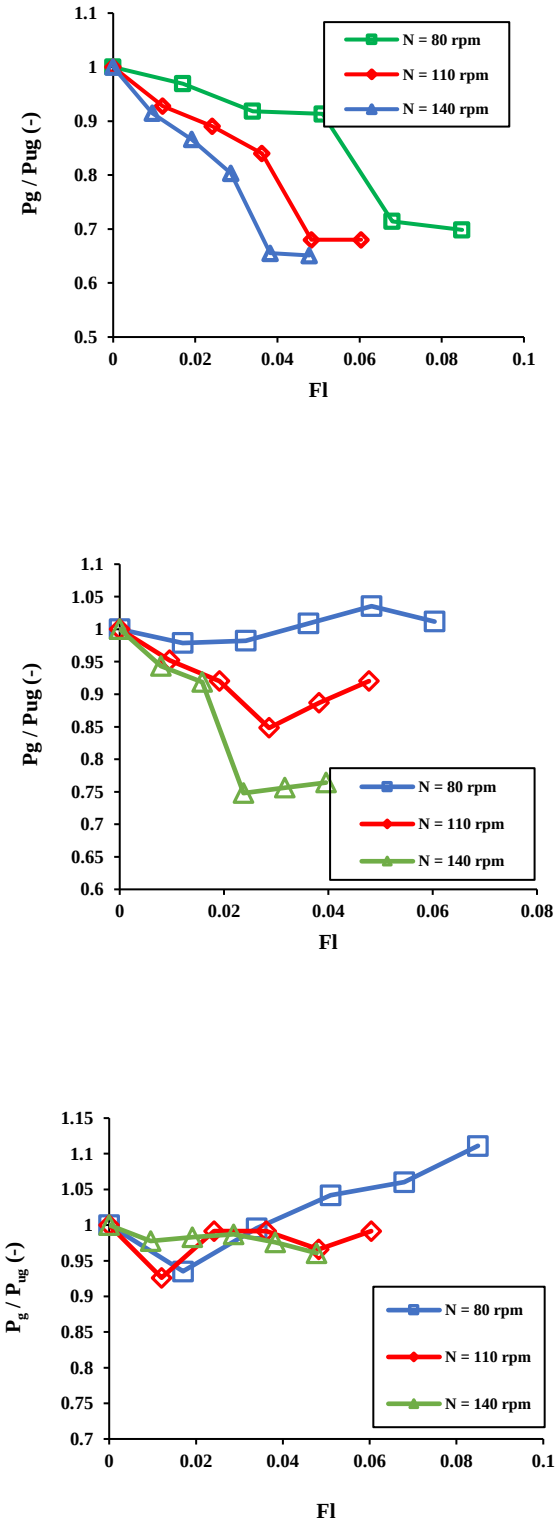

Fig. 6: P_g/P_{ug} versus flow number (Fl) at different impeller speeds for an air-water system equipped with: (a) Rushton turbine, (b) downward PBT, and (c) ASI impeller.

Fig. 6b shows the relative power consumption curve as a function of flow number for the PBT at three different impeller speeds which are the same as those employed for the Rushton impeller. This figure shows complex behavior of P_g/P_{ug} for the PBT. In comparison, at a low impeller speed of N = 80 rpm (Fr = 0.035), the PBT maintained a much higher relative power than those attained at two other speeds. P_g/P_{ug} increased with increasing the flow number, and the power drawn under the gassed condition was slightly higher than that drawn under the equivalent ungassed condition. Similar behavior was reported by other researchers for axial impellers (*Bakker* and *Van den Akker* 1994*; McFarlane* and *Nienow* 1996*; Arjunwadkar et al.* 1998*; Myers et al.* 1999*; Woziwodzki* and *Broniarz* 2014*; Kaiser et al.* 2017). These were shown by the existence of small bubbles in the vortex zone behind the blades that disturb and separate the boundary layer of flow, and cause the increase in drag and power consumption (*McFarlane* and *Nienow*, 1996).

At N = 110 rpm (Fr = 0.073), the relative power shows a steep decrease at a gas flow number between 0.01 and 0.03 and it increased at $Fl \geq 0.03$. At N = 140 rpm (Fr = 0.120), P_g/P_{ug} curve for PBT shows a steep decrease at $0.02 \leq Fl \leq 0.04$ and then increased at a flow number more than 0.04. Previous researchers have reported the same complex behaviors for the downward pumping PBT (*Bakker* and *Van den Akker* 1994*; Paul et al* 2004).

Indeed, for the PBT impeller at lower gas rates ($Fl \leq 0.02$) and high impeller speeds (N=110 rpm and N = 140 rpm), due to a strong downward flow created by impeller, the input gas from the sparger entered the impeller zone from the top of the impeller and was pushed down from the bottom; this is known as the indirect loading *(Paul et al* 2004*)*. At higher gas flow rates ($Fl \geq 0.03$), the gas was directly loaded to the impeller zone from the beneath of the impeller and thus the impeller pumped the fluid radially (*Paul et al.* 2004). So, for the downward-pumping PBT impeller, both the direct and indirect loading regimes were identified in aerated mixing system (*Warmoeskerken et al.*, 1984*; Bakker* and *Van den Akker* 1994*; Paul et al* 2004), which resulted in a complex behavior of this impeller under the aeration.

In Fig. 6c, the relative power consumption curve is sketched as a function of the flow number for the ASI impeller, using the same three constant impeller speeds used with the two other impellers. This figure shows that at a low impeller speed (N=80 rpm), when the gas flow

number was more than 0.04, P_g/P_{ug} increased with the increasing flow number. It means that the power drawn in the aerated condition was more than that drawn under the equivalent un-aerated condition. This behavior was similar to that observed for the axial-flow PBT impeller as depicted in Fig. 6b. This trend of P_g/P_{ug} changed at the higher impeller speeds. At N = 110 rpm and $Fl \geq 0.02$, a small reduction of relative power consumption was observed and at N =140 rpm, this parameter was approximately constant and did not change with the gas flow number. In a complete dispersion condition, power consumption is independent of gas flow rate and impeller speed (*Nienow*, 1998*; Gabelle et al.*, 2011*)*. Thus, it can be concluded that for the wide ranges of flow number and impeller speed, the gassed to ungassed power ratio for the ASI impeller did not change significantly and a complete dispersion regime was achieved. This was due to the special blades shape of the ASI impeller, which led to a complete and uniform recirculation of bubbles in this range of operational conditions. The similar results were also attained for the gas dispersion in non-Newtonian fluids with the ASI impeller *(Khalili et al.*, 2017a*)*. This behavior is highly desirable in industry especially for bioreactors (*Macfarlane* and *Nienow*, 1996). Another impeller that exhibits a similar behavior is the Up-pumping Elephant Ear (EEU) agitator. For the EEU impeller, under any aeration rate, $P_g/P_{ug} \approx 1$ (*Zhu et al., 2009*). However, in spite of this great advantage, Zhu et al. (2009) reported that the measured air hold-up was small for this impeller.

To compare the hydrodynamic performance of the ASI impeller with the downward PBT, and the Rushton turbine, a plot of the relative powers drawn versus gas flow rate was made; it compares them at equal specific ungassed power input of 200 W/m^3 and the results are shown in Fig. 7.

This figure shows that the power drawn under gassed operation by the Rushton turbine shows a reduction of approximately 50% compared to its un-gassed value. The power drawn by the downward PBT shows a greater dependency on speed and the maximum reduction of power drawn was 22% of the ungassed condition. The ASI impeller shows more stable relative power drawn compared to the other impellers over the domain of operating conditions in this study. From Fig. 7 it can be seen that the ASI impeller could be about 45% more efficient than the Rushton turbine and 20% more than the downward PBT under the operating conditions employed

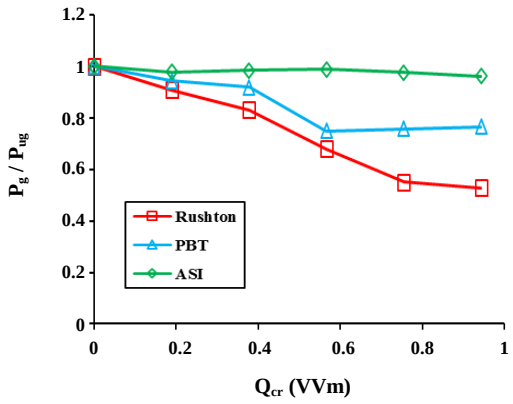

Fig. 7: P_g/P_{ug} versus the gas flow rate for the air-water systems agitated by the ASI impeller, downward PBT and the Rushton turbine at P = 200 w/m^3.

in this study (i.e. Q_g about 1 vvm). The capability of the ASI impeller to preserve a higher relative power drawn at aerated condition is a benefit to the industry.

Until now many correlations have been proposed in the literature for the estimation of the relative power consumption (P_g/P_{ug}) for the mono-impeller systems and multi- impeller systems *(Luong* and *Volesky*, 1979*; Hudcova et al., 1989; Abrardi et al.*, 1990*; Bouaifi et al.*, 2001*; Bouaifi* and *Roustan* 2001*; Paul et al.*, 2004*)*. Despite the great amount of data, it is difficult to find a single equation that is accurate for any aerated system. Table 2 lists some of the proposed correlations for standard vessels with single impellers. Recently there has been a tendency to use a dimensionless correlation due to its importance for the scale up of aerated mixing systems (*Gabelle et al., 2011; Gill et al., 2008; Kadic and Heindel, 2010).* Previous research and our experimental data show that the ratio of gassed power to the ungassed power consumption is proportional to the gas flow number and Froude number. In this study, the proposed correlation by Fujisova et al. (2007) (Eq. (8)) was employed:

$$\frac{P_g}{P_{ug}} C_1 Fl_g^{C_2} Fr^{C_3} \quad (8)$$

In this equation, C_2 shows the influence of the gas flow rate and C_3 represents the effect of the impeller speed, all of which are affected by the geometry of the impeller. The higher value of C_3 may be attributed to the vortex formed in the center of the tank (*Xie et al.*, 2014*; Fujisova et al.*, 2007*; Gabelle et al.*, 2011*; Gill et al.*, 2008).

Table 2: Correlations reported in the literature for the gassed to un-gassed power consumption (P_g/P_{ug}) of stirred vessels.

References	Vessel Diameter (m)	Proposed Correlation
Cui et al. (1996)	0.23–1.83 $(\frac{QN^{0.25}}{d_i^2}) \leq 0.055$ $(\frac{QN^{0.25}}{d_i^2}) \geq 0.055$	$1-\frac{P_g}{P_{ug}} = 9.9\,(\frac{QN^{0.25}}{d_i^2})$ $1-\frac{P_g}{P_{ug}} = 0.52 + 0.62\,(\frac{QN^{0.25}}{d_i^2})$
Mockel et al. (1990)	0.4–7	$\frac{P_g}{P_{ug}} = \frac{1}{\sqrt{1+Z\,\frac{u_s}{g d_T}}}$
Gabelle et al. (2011)	all configuration	$ln(\frac{P_g}{P_{ug}}) = -15.36\,Q_g^{0.62}T^{-1.7}\left(\frac{D}{T}\right)^{0.51} Np^{0.16}$
Fujasova et al., (2007)	all configuration	$\frac{P_g}{P_{ug}} = C_1 Fl_g^{C_2} Fr^{C_3}$
Xie et al., (2014)	all configuration	$\frac{P_g}{P_{ug}} = C_1 Fl_g^{C_2} Fr^{C_3} Re^{C_4}$

Table 3. Reported empirical coefficients of Eq. 8 for an air-water agitated system and the coefficients obtained in this study for the ASI impeller, the downward PBT and the Rushton turbine.

Impeller	C_1	C_2	C_3	SD (%)	Reference
Rushton	0.0476	-0.37	-0.126	12.8	Fujasova et al., 2007
	0.1	-0.25	-0.2	11.5	Hughmark et al., 1980
	0.126	-0.319	-0.207	10.4	Xie et al., 2014
	0.33	-0.313	0.07	30.4	This work
PBT	0.111	-0.245	-0.144	26.4	Fujasova et al., 2007
	1	0.1	-0.1	12.2	This work
ASI	1.5	0.0653	-0.03	6.7	This work

Using the experimental data obtained in this work, the parameters C_1, C_2 and C_3 were calculated for each impeller by the regression method. Calculated parameters in this study along with the parameters reported by other researchers are presented in Table 3.

As can be seen in this table, the exponent C_2 for the Rushton turbine is smaller than the other two impellers; this confirmed that the power drop of this impeller is most obviously the result of aeration. The exponent C_2 for the ASI is greater than the two other mixers, which indicates the power drop of the ASI is very low under the gassed conditions. The predicted power ratio shown in Eq. (8) has been compared by the experimental power ratios in Fig. (8). As shown in this figure, this correlation can predict relative power consumption with an error margin of ± 0.22.

To analyze the effect of the rotational speed of the impeller on gassed power consumption, the gassed power number as a function of the rotational speed, at a constant volumetric gas flow rate of 0.0002 m^3/s (0.1887 vvm) was generated for the ASI impeller, downward PBT and the Rushton turbine. The results are illustrated in Fig. 9. As can be seen from this figure, for all three impellers, the power number had the higher value at low speeds and fell steeply when the impeller speed was increased from 25 rpm (Fr = 0.003) to 50 rpm (Fr = 0.02). It has been stated that at low rotational impeller speeds, the rising of gas bubbles in the vessel opposes the impeller pumping action (*McFarlane and Nienow 1996; Kaiser et al. 2017*). In this operating condition, due to the attachment of the bubbles to the back of the blades and the formation of large cavities, a meaningful decrease in impeller pumping capacity and power consumption can be seen (*Gabelle et al.* 2011*; McFarlane* and *Nienow* 1996). Also this figure shows that in each impeller speed, the gassed power number of the Rushton turbine was higher than the other impellers, and the PBT had the lowest power number.

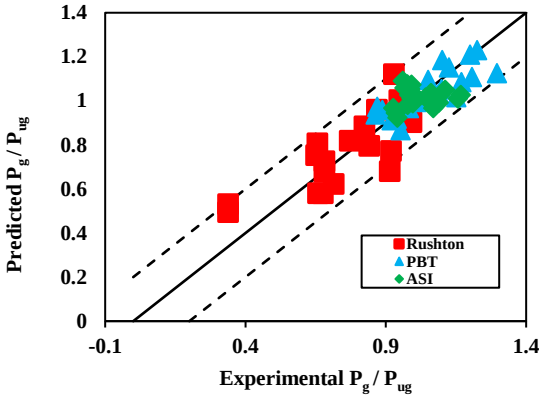

Fig. 8: Predicted P_g/P_{ug} from Eq. 8 versus the experimentally measured P_g/P_{ug}.

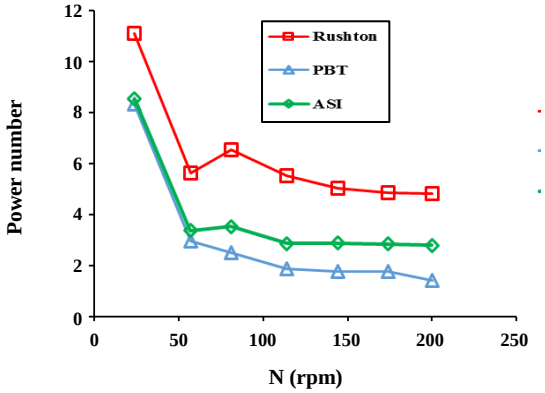

Fig. 9: Gassed power number (Np) versus the impeller speed for the ASI impeller, downward PBT and The Rushton turbine at Q_g = 0.0002 m^3/s.

The Rushton impeller is a radial-flow impeller and the PBT is an axial-flow impeller, and the power number of the radial-flow impellers is greater than for the axial-flow impellers. The power number of the ASI impeller (a radial-axial flow impeller) was between these two.

For the radial Rushton impeller, the power number increased by increasing the impeller speed from 50 rpm (Fr = 0.02) to 80 rpm (Fr = 0.035) because the flow pattern changes from flooding to loading regime in this range of operating condition (*Gabelle et al., 2011*). Increasing the impeller speed from 80 rpm causes a continuous decrease in the power number due to an increase in the cavity size behind the impeller blades *(Nienow,* 1998).

For the ASI impeller, the gassed power number stayed constant except when the impeller speed was lower than 110 rpm ($Fr \leq 0.07$). This velocity was the minimum speed for the complete dispersion regime for this impeller. The changes in the power number for this impeller for the impeller rotational speeds between 50 rpm to 110 rpm was due to the change of flow pattern from complete dispersion to the loading condition.

For the axial-flow PBT at the impeller speeds more than 50 rpm, the gassed power number continued to decline with increasing the rotational speed of the impeller, due to larger increases in cavity size and recirculation (*McFarlane et al.*, 1995).

Gas Holdup

One of the most important parameters for gas-liquid stirred tank reactors is gas holdup, which depends on the gas flow rate, the liquid properties and impeller geometry (*McFarlane et al.*, 1995*; vasconcelos et al.*, 2000*; Moucha et al.*, 2003*)*. The liquid flow pattern has a major effect on overall gas holdup. This parameter would increase when the gas is effectively dispersed, or the rotational speed of the impeller or the gas flow rate is increased (*McFarlane et al.*, 1995; *Moucha et al.*, 2003).

In order to study the influence of the aeration rate, in Fig. 10 the measured data of gas holdup are plotted as a function of the gassed specific power input for the ASI impeller at different superficial gas velocities. As can be seen from this figure, in low gas velocity of V_s = 1.6 m/s, the increase in power consumption from 14.32 W/m^3 to 42.81 W/m^3 resulted in the increase in gas holdup from 0.2% to 0.3%; more increases in power consumption did not have any effect on gas holdup. At larger gas velocities, the gas holdup increased continuously by increasing the power consumption, and hold up increased to 1.8% at V_s = 8.3 m/s when power consumption increased to 197.07 W/m^3. Indeed for the low gas velocity of V_s = 1.6 m/s, the impeller power consumption around 42.81 W/m^3 was powerful enough to break the bubbles and thus the complete gas dispersion was achieved in the system. At the higher gas velocity, more specific power input resulted in the breakage of the larger bubbles to the smaller size. The formation of these small bubbles with the longer residence time resulted in a higher gas holdup throughout the vessel (*Hashemi et al.*, 2016; *Macfarlane* and *Nienow*, 1996). In Fig. 10, as expected, at a fixed impeller power consumption, the overall gas holdup increased

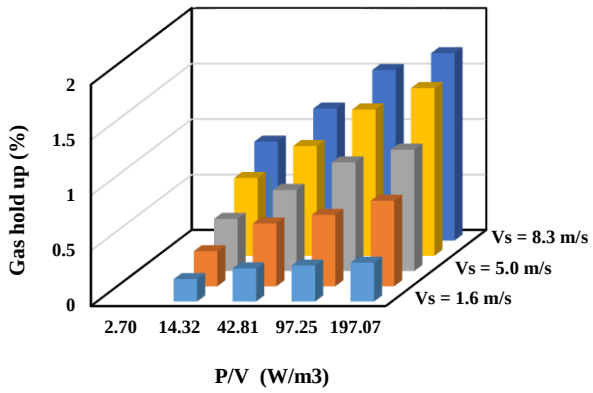

Fig. 10: Gas holdup versus specific power consumption in an aerated tank equipped with the ASI impeller at different superficial gas velocities.

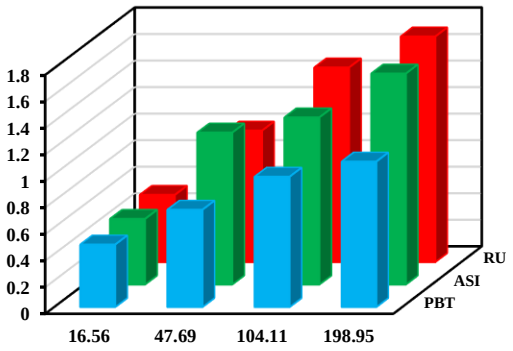

Fig. 11: Gas holdup versus specific power consumption at Q_g = 0.0005 m^3/s for the agitated tanks equipped with the ASI impeller, downward PBT and the Rushton turbine.

by increasing the superficial gas velocity. The higher superficial gas velocity means more bubbles in the tank and that causes a higher gas holdup.

In order to compare the hydrodynamic performance of the newly designed ASI impeller with the Rushton turbine and the downward PBT, a plot of the obtained data for gas holdup as a function of gassed specific power input, at a superficial gas velocity equal to 0.0005 m^3/s, was generated and is displayed in Fig. 11. At a low power input when $16.56 \leq P/V \leq 104.11$ W/m^3 ($0.03 \leq Fr \leq 0.07$), the overall gas holdup attained by the ASI impeller was higher than those for the Rushton turbine and the downward PBT. However, at the high power input when $P/V > 104.11$ W/m^3 ($Fr > 0.07$) in this study, the Rushton turbine generated the higher gas holdup, and the downward PBT created a lower gas holdup at a fixed power input. This is in agreement with previous studies reported that the gas holdups produced by the radial-flow impellers are higher than those achieved by the axial-flow impellers *(Moucha et al.,* 2003*; Fujasova et al.,* 2007*)*. The amount of gas holdup produced by the ASI impeller (see Fig. 11) was between the generated gas holdup by the Rushton turbine and the PBT impeller. The same behavior was seen for this impeller in the gas dispersion in non-Newtonian fluids *(Khalili et al.,* 2017a*; Khalili et al.,* 2017b*)*.

According to Bujalski's 1986 approach, the gas holdup can be expressed as a function of impeller power consumption and superficial gas velocity *(McFarlen et al., 1995)*:

$$\varepsilon = \alpha \left(\frac{P_g}{V_L}\right)^{\beta} V_s^{\gamma} \qquad (11)$$

In this equation α, β and γ are the numerical coefficients related to the impeller geometry. Correlation (11) is helpful as a way to compare the performance of various impellers with different power numbers *(Gabelle et al.,* 2011*; Hashemi et al., 2016; Moucha et al.,* 2003*; McFarlen et al.,* 1995*; Vasconcelos et al.,* 2000*)*. The experimental data collected in this study were utilized to calculate the values of α, β and γ through the regression method and are given in Table 4 for the ASI impeller, the downward PBT, and the Rushton turbine along with some of the coefficients provided by other researchers for comparison. As shown in Fig. 12, the proposed correlation can estimate the gas holdup percentage with an error margin of ± 0.5%. What is notable is that the majority of predicted data show high accuracy.

Mixing Time

Mixing time is another parameter that is very important when comparing stirred tanks (*Vrabel et al., 2000)*. The mixing time is a function of impeller speed, power consumption, and gas flow rate in a gas–liquid stirred tank (*Kadic and Heindel, 2010*; *Gabelle et al., 2011; Ascanio, 2015; Bouaifi and Roustan, 2001; Vasconcelos et al., 2000*).

A plot of mixing time as a function of specific power consumption for the ASI impeller, the Rushton turbine and downward PBT was created to investigate and clarify the effect of power consumption and gas flow rate on the mixing time. This is shown in Fig. 13 for two gas flow rates (Q_g = 0.0002 m^3/s and Q_g = 0.0003 m^3/s).

Table 4: Reported empirical coefficients for the gas holdup correlation (Eq. 13) and those coefficients obtained in this work for the ASI impeller, the downward PBT and the Rushton turbine.

Impellers	α	β	γ	SD	R^2	References
Rushton	0.016	0.62	0.56	0.78	0.95	Moucha et al., (2003)
	0.493	0.24	0.99			McFarlen et al., (1996)
	1	0.37	0.65			Vasconcelos et al., (2000)
	0.040	0.32	1.14			This work
PBT	0.046	0.46	0.58	0.78	0.86	Moucha et al., (2003)
	0.031	0.56	0.87			This work
ASI	0.053	0.29	0.92	0.62	0.98	This work

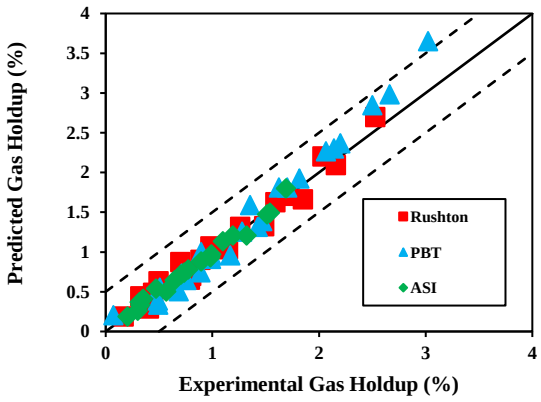

Fig. 12: Predicted gas holdup from Eq. 11 versus the experimental gas holdup.

Fig. 13a depicts mixing time versus power consumption for the Rushton turbine. According to this figure, it was found that for P/V < 25 W/m^3, mixing time decreased rapidly as the power consumption increased. For 25 ≤ P/V ≤ 75, the mixing time decreases with less intensity and for P/V ≥ 75 W/m^3, an increase in the power consumption had no more effect on the mixing time. This behavior is due to the changes of flow regime from flooding (P/V < 25) to complete gas dispersion system (P/V ≥ 75).

This figure also shows that when P/V ≥ 25 W/m^3, an increase in the gas flow rate from 0.0002 m^3/s to 0.0003 m^3/s had no effect on the mixing time. Indeed under this operating condition, the influence of the flow produced by the impeller overcame the effect of the flow generated by the upward gas bubbles. It is clear that changes in the gas flow rate had no effect on mixing time.

The plot of mixing time versus power consumption for the PBT impeller is shown in Fig. 13b. It can be seen that mixing time decreased as the power consumption for each two gas flow rates increased. However, at Q_g = 0.0003 m^3/s for P/V ≥ 65 W/m^3, the mixing time did not change when the power consumption increased. This figure shows that at Q_g = 0.0003 m^3/s, the mixing time was smaller than Q_g = 0.0002 m^3/s because of the better mixing achieved at the higher gas flow rate.

As can be seen from Fig. 13c, for the radial-axial ASI impeller, mixing time decreased by increasing the power consumption at each gas flow rate. At P/V≤ 100 W/m^3, mixing time decreased by increasing the gas flow rate at equal power consumption because the upward gas flow created additional mixing especially at the higher gas flow rate. At P/V >100 W/m^3, changes in the gas flow rate from Q_g = 0.0002 m^3/s to Q_g = 0.0003 m^3/s had no effect on the mixing time; this showed that the agitation produced by the impeller dominated the upward movement of bubbles.

From the experimental data shown in Fig. 13, it is obvious that when the impeller power consumption is between 80 w/m^3 to 350 w/m^3 (which is equivalent to the conditions that 0.03 ≤ Fr ≤ 0.07), in each gas flow rate the Rushton turbine shows a lower mixing time with a higher power consumption compared to the other mixer. Although at a lower impeller speed, the mixing time of the Rushton turbine is much greater than the two other mixers.

Generally, the mixing efficiency $P_g.t_{mg}$ is used as a common scale for comparison of different gas-liquid mixing systems. By this definition, it is obvious that better mixing efficiency is related to the lower energy consumption and mixing time *(Bouaifi* and *Roustan*, 2001*; Rivera et al.*, 2006*)*. In this study, $\frac{1}{P_g.t_{mg}}$ was calculated for the ASI impeller, Rushton turbine, and downward PBT at different flow numbers and a constant rotational speed equal to 140 rpm. The results are reported in Fig. 14. As shown in this figure, the axial downward PBT provided

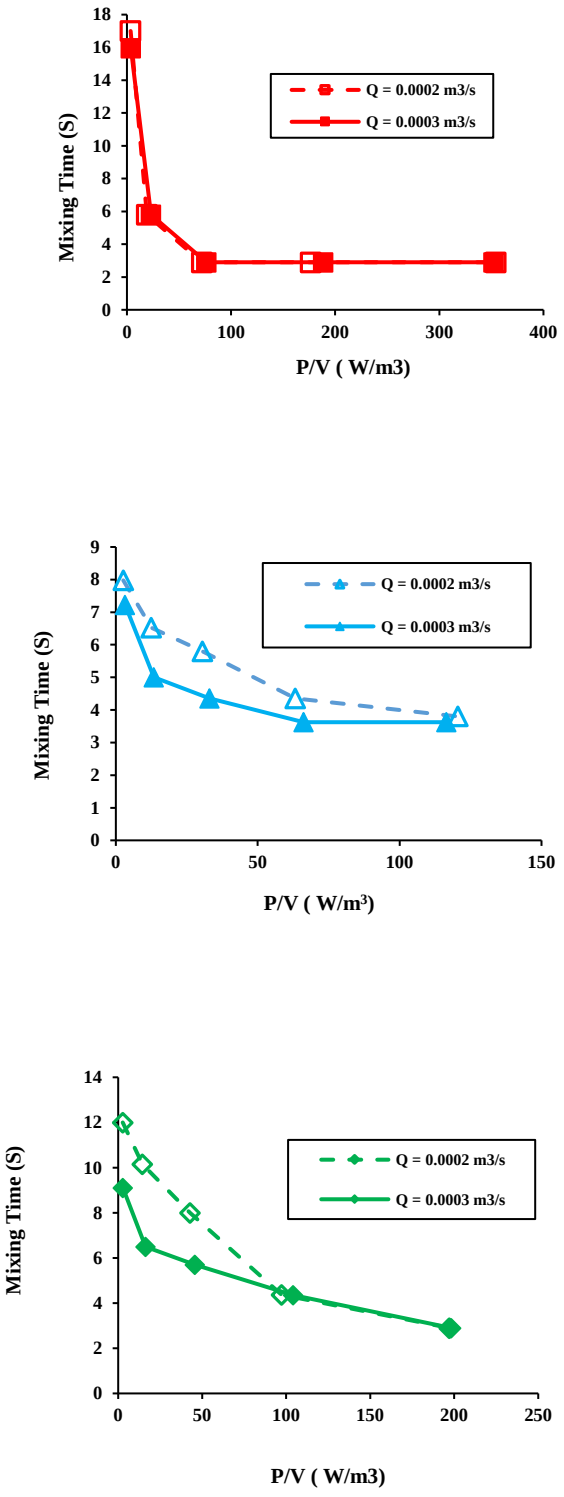

Fig. 13: Mixing time versus specific power consumption at two gas flow rates for the (a) Rushton impeller, (b) downward PBT, and (c) ASI impeller.

the best mixing performance, which is related to lower homogenization energy, and the Rushton turbine presented the worst performance. The effect of gas flow rate on mixing efficiency revealed a better mixing performance at higher gas flow rates- than for the lower ones- for the downward PBT and the Rushton turbine. The axial-radial ASI impeller shows a special result in this figure. The ASI impeller gave the same performances at all gas flow rates investigated in this study. The special behavior of the mixing curve for the ASI impeller can be explained by referring to its gassed power behavior**,** which indicated that the changes of gas flow rate had little effects on the power consumption of this impeller.

Although Fig. 14 shows tha**t** the downward PBT had a better mixing efficiency in comparison with the other impeller in this work, the gas holdup attained by the PBT was less than those achieved by the Rushton and the ASI impeller. The power of the PBT also decreased under the aeration by 22% compared to that for the ASI impeller.

CONCLUSIONS

Electrical resistance tomography was used to investigate the hydrodynamics of two- phase gas-liquid mixing system in a stirred vessel equipped with a newly designed ASI impeller, and the achieved results were compared with the downward PBT and the Rushton turbine impellers. The assessment was carried out with respect to the mixing time, power consumption and gas holdup under similar aeration conditions. The collected data indicate the following significant results:

1- It was found that power consumption under aeration condition was almost constant with an increasing gas flow rate at constant impeller speed when the mixing system was equipped with the ASI impeller.

2- An investigation into the effect of agitation speed on (P_g/P_{ug}) for the ASI impeller demonstrated that the aerated power consumption changed little with an increase in impeller speed at constant gas flow rate.

3- The empirical coefficient for the dimensionless correlation of P_g/P_{ug}, was calculated by using the experimental data.

4- The empirical coefficient of dimensionless power law correlation for gas holdup, as a function of specific power consumption and gas velocity, was calculated.

5- The highest gas holdup at constant power consumption for the ASI impeller, in comparison to the Rushton

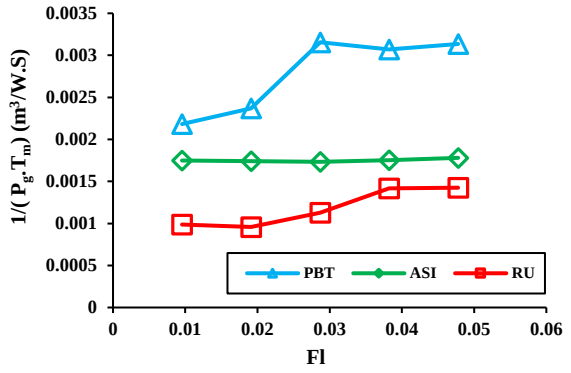

Fig. 8: Predicted P_g/P_{ug} from Eq. 8 versus the experimentally measured P_g/P_{ug}.

turbine and downward PBT impeller, revealed that the ASI impeller was an effective impeller compared to the others in lower power input when $P/V \leq 104.11$ W/m^3 ($Fr \leq 0.07$).

6- It was found that the mixing time of the ASI impeller decreased with increases in rotational speed and it was a function of gas flow rate when $P/V \leq 100$ ($Fr \leq 0.07$) in the aerated system. However, for $P/V > 100$ ($Fr > 0.07$), the mixing time showed no significant changes with increasing the gas flow rate and power input.

7- Overall conclusion of the mixing time, power consumption and gas holdup results showed that the axial-radial ASI impeller is a good energy efficient impeller for the aeration system and bioreactors.

Nomenclature

D	Impeller diameter, m
Fl	Flow number, $Fl=Q_g/(ND^3)$, dimensionless
Fr	Froud number , $Fr= N^2D/g$
H	Height of fluid in vessel, m^3
M	Torque
N	Impeller rotational speed, round/s
N_p	Power Number, $Np = \frac{P}{\rho N^3 D^5}$, Dimensionless
P	Power consumption, $p = 2\pi NM$, W
P_{tot}	Total power, W
P_g	Power in gassed condition, W
P_{ug}	Power in ungassed condition, W
Q_g	Gassed flow rate, m^3/s
Q_{GV}	Specific gas flow rate, m^3/s
Re	Impeller Reynolds, $Re = \frac{\rho N D^3}{\eta}$, Dimensionless
T	Time, s
t_m	Mixing time, s
T	Tank dimension, m
V	Fluid volume, m^3
Vs	Superficial gas velocity, m/s
vvm	(volumetric gas flow rate/min)/volume of liquid
X	Sign for different variables
X_i	Sign for different variables
ρ	Fluid density, kg/m^3
μ	Viscosity, Pa.s
τ	Yeld stress, Pa
μ_0	Yield viscosity, Pa.s
σ_0	Conductivity of gas phase, µs/cm
σ	Conductivity of liquid phase µs/cm
g	Gravitational acceleration, m/s^2

Received : Aug.. 28, 2019 ; Accepted :Nov. 18, 2019

REFERENCES

[1] Abrardi V., Rovero G., Baldi G., Sicardi S., Conti R., Hydrodynamics of a Gas-Liquid Reactor Stirred with a Multi-Impeller System, *Chem. Eng. Res. And Des*., **68**: 516-522 (1990).

[2] Arjunwadkar S.J., Saravanan K., Pandit A.B., Kulkarni P.R., Optimizing the Impeller Combination for Maximum Hold-Up with Minimum Power Consumption, *Biochem. Eng. J*., 1: 25-30 (1998).

[3] Ascanio G.A., Mixing Time in Stirred Vessels: A Review of Experimental Techniques, *Chinese Journal of Chemical Engineering*, **23**: 1065–1076 (2015).

[4] Bakker A., Van Den Akker H.E.A., Single-Phase Flow in Stirred Reactors, *Chem. Eng. Res. and Des., Trans Ichem E.*, **72**: 583-593(1994).

[5] Bouaifi M., Roustan M., Power Consumption, Mixing Time and Homogenization Energy in Dual-Impeller Agitated Gas-Liquid Reactors, *Chem. Eng. And Processing*, **40**: 87–95 (2001).

[6] Bouaifi M., Hebrard G., Bastoul D., Roustan M., Comparative Study of Gas Hold-Up, Bubble Size, Interfacial Area and Mass Transfer Coefficients in Stirred Gas-Liquid Reactors and Bubble Columns, *Chem. Eng. and Processing*, **40**: 97–111 (2001).

[7] Boyer, C., Duquenne, A.M., Wild, G., Measuring Techniques in Gas-Liquid and Gas-Liquid-Solid Reactors, *Chem. Eng. Sci.*, **57** (16): 3185–3215 (2002).

[8] Dong F., Jiang Z.X., Qiao X.T., Xu L.A., Application of Electrical Resistance Tomography to Two-Phase Pipe Flow Parameters Measurement, *Flow Measurement and Instrumentation*, **14**: 183–192 (2003).

[9] Znicova, M., Linek, V., Moucha, T., Mass Transfer Correlations for Multiple Impeller Gas-Liquid Contactors. Analysis of the Effect of Axial Dispersion in Gas and Liquid Phases on "Local" K_la Values Measured by the Dynamic Pressure Method in Individual Stages of Vessel, *Chem. Eng. Sci.*, **62**: 1650-1669 (2007).

[10] Gabelle J.C., Augier F., Carvalho A., Rousset R., Morchain J., Effect of Tank Size on Kla and Mixing Time in Aerated Stirred Reactors with Non-Newtonian Fluids, *Can. J. Chem. Eng.*, **9999**: 1-15 (2011).

[11] Gill N.K., Appleton M., Baganz F., Lye G.J., Quantification of Power Consumption and Oxygen Transfer Characteristics of a Stirred Miniature Bioreactor for Predictive Fermentation Scale-Up, *Biotech. Bioeng.*, **100**(6): 1144–1155 (2008).

[12] Hashemi N., Ein-Mozaffari F., Upreti S.R., Huwang D.K., Analysis of Mixing in Aerated Reactor Equipped with the Coaxial Mixer Through Electrical Resistance Tomography and Response Surface Method, *Chem. Eng. Res. and Des.*, **109**: 734-752 (2016).

[13] Harnby N., Edwards M.F., Nienow A.W., "Mixing in the Process Industries", Second Edition, (1997).

[14] Hudcova V., Machon V., Nienow A.W., Gas-Liquid Dispersion with Dual Rushton Turbine Impellers, Biotec. Bioeng., **34**(5): 617–628 (1989).

[15] Kadic E., Heindel T.J., Mixing Considerations in Stirred Tank Bioreactors When Using Fluid Property Altering Microorganisms. Mechanical Engineering Conference Presentations, *Papers and Proceedings*, Paper 121 (2010).

[16] Kaiser S.C., Werner S., Kraume, M., Eibl D., Development of a Method for Reliable Power Input Measurements in Conventional and Single-Use Stirred Bioreactors at Laboratory Scale, *Eng. Life Sci.*, **17**: 500–511 (2017).

[17] Khalili F., Jafari Nasr M.R., Kazemzadeh A., Ein-Mozaffari F., Hydrodynamic Performance of the ASI Impeller in an Aerated Bioreactor Containing the Biopolymer Solution Through Tomography and CFD, *Chem. Eng. Res. and Des.*, 125: 190–203 (2017a).

[18] Khalili F., Jafari Nasr M.R., Kazemzadeh A., Ein-Mozaffari, F., Analysis of Gas Holdup and Bubble Behavior in a Biopolymer Solution Inside a Bioreactor Using Tomography and Dynamic Gas Disengagement Techniques, *J. Chem. Technol Biotechnol*, (Wileyonlinelibrary.Com) DOI 10.1002/Jctb.5356 (2017b).

[19] Khare A.S., Niranjan K., The Effect of Impeller Design on Gas Hold-Up in Surfactant Containing Highly Viscous Non-Newtonian Agitated Liquids, *Chem. Eng. Proc.*, **41**: 239–249 (2002).

[20] Luong H.T., Volesky B., Mechanical Power Requirements of Gas-Liquid Agitated Systems, *Aiche J.*, 25(5): 893–895 (1979).

[21] Mcfarlane C.M., Zhao X., Nienow A.W., Studies of High Solidity Ratio Hydrofoil Impellers for Aerated Bioreactors. 2. Air-Water Studies, *Biotechnology Progress*, 11: 608-618 (1995).

[22] Mcfarlane C.M., Nienow A.W., Studies of High Solidity Ratio Hydrofoil Impellers for Aerated Bioreactors. 4. Comparison of Impeller Types, *Biotechnology Progress*, 12: 9-15 (1996).

[23] Michel B.J., Miller S.A., Power Requirements of Gas-Liquid Agitated Systems, *Aiche J.*, **8**(2): 262–266 (1962).

[24] Montante G., Paglianti A., Gas Hold-Up Distribution and Mixing Time in Gas-Liquid Stirred Tanks, *Chem. Eng. J.*, **279**: 648–658 (2015).

[25] Moucha T., Linek V., Prokopovoa E., Gas Hold-Up, Mixing Time and Gas–Liquid Volumetric Mass Transfer Coefficient of Various Multiple-Impeller Configurations: Rushton Turbine, Pitched Blade and Techmix Impeller and Their Combinations, *Chem. Eng. Sci.*, **58**(9): 1839-1846 (2003).

[26] Myers K.J., Thomas A., Bakke, A., Reeder M.F., Performance of a Gas Dispersion Impeller with Vertically Asymmetric Blades, *Chem. Eng. Res. and Des.*, **77**(8): 728-730 (1999).

[27] Nienow A.W., Hydrodynamics of Stirred Bioreactors, *Applied Mechanics Reviewers*, **51**: 3-31 (1998).

[28] Paglianti, A., Takenaka, K., Bujalski, W., Simple Model for Power Consumption in Aerated Vessels Stirred by Rushton Disc Turbines, *Aiche J.*, **47**(12): 2673-2683 (2001).

[29] Pakzad L., Ein-Mozaffari F., Upreti S.R., Lohi A., A Novel and Energy-Efficient Coaxial Mixer for Agitation of Non-Newtonian Fluids Possessing Yield Stress, *Chem. Eng. Sci.*, **101**: 642-654 (2013).

[30] Pakzad L., Ein-Mozaffari F., Chan P., Using Electrical Resistance Tomography and Computational Fluid Dynamics Modeling to Study the Formation of Cavern in the Mixing of Pseudo Plastic Fluid Possessing Yield Stress, *Chem. Eng. Sci*., **63**: 2508-2522 (2008).

[31] Paul E.L., Atiemo-Obeng V.A., Krestal S. M., "Hand Book of Industrial Mixing. Science and Practice", Wiley–Inter Science, USA (2004).

[32] Pignaton R., Rogério L., Otávio L., Junior Applying A Parallel Solution to the Graph Partitioning Problem in the Simulation of Multiphase Flows, *Iran. J. Chem. Chem. Eng. (IJCCE)*, **3**(2): 87-92 (2014).

[33] Rivera C., Foucault S., Henche M., Espinsoa-Slares T., Tanguy P.A., Mixing Analysis in a Coaxial Mixer, *Chem. Eng. Sci*., **61**(9): 2895-2907 (2006).

[34] Tatterson G.B., Kyser E.A., Mixing in Fed-Batch and Continuous Flow Processes in Nonstandard Geometries, *Aiche J.* Wiley Online Library, (1991).

[35] Taleshi Ahangari H., Noeparvar P., Moghaddas J.S., The Effect of Impeller Type on The Mixing Time of the Non-Newtonian Fluids in Stirred Tanks, *CTAIJ.*, **11**(4): 123-132 (2016).

[36] Vasconcelos J.M.T., Orvalho S.C.P., Rodrigues A.M.A.F., Alves S.S., Effect Of Blade Shape on the Performance of Six-Bladed Disk Turbine Impellers, *Ind. Eng. Chem. Res.*, **39**(1): 203–213 (2000).

[37] Vlaev, S. D., Valeva, M. D., Mann, R., Some Effects of Rheology on The Spatial Distribution of Gas Hold-up in a Mechanically Agitated Vessel, *Chem. Eng. J.*, **87**: 21-30 (2002).

[38] Vrábel P., Van Der Lans R.G.J.M., Luyben K.C.A.M., Boon L., Nienow A.W., Mixing In Large Scale Vessels Stirred with Multiple Radial or Radial and Axial Up-Pumping Impellers: Modelling and Measurements, *Chem. Eng. Sci.*, **55** (23): 5881–5896 (2000).

[39] Wang M., Dorward A., Vlaev D., Mann R., Measurements of Gas-Liquid Mixing in a Stirred Vessel Using Electrical Resistance Tomography (ERT), *Chem. Eng. J.*, **77** (1-2): 93–98 (2000).

[40] Woziwodzki S., Broniarz-Press L., Power Characteristics of Unsteadily Rotating Rushton Turbine in Aerated Vessel, *Technical Transactions*, 2-Ch (2014).

[41] Xie M.H., Xia J.Y., Zhou Z., Zhou G.Z., Chu J., Zhuang Y.P., Zhang S., Noorman H., Power Consumption, Local and Average Volumetric Mass Transfer Coefficient in Multiple Impeller Stirred Bioreactors for Xanthan Gum Solutions, *Chem. Eng. Sci*., **106**: 144–156 (2014).

[42] Zhang Q., Yong Y., Mao, Z.S., Yang, C., Zhao C., Experimental Determination and Numerical Simulation of Mixing Time in a Gas-Liquid Stirred Tank, *Chem. Eng. Sci*., **64** (12): 2926 – 2933 (2009).

[43] Zhu H., Nienow A.W., Bujalski W., Simmons M.J.H., Mixing Studies in a Model Aerated Bioreactor Equipped with an Up-Or a Down-Pumping 'Elephant Ear'- Agitator: Power, Hold-Up and Aerated Flow Field Measurements, *Chem. Eng. Res. Des*., **87**(3): 307–317 (2009).

[44] "P2+ Electrical Resistance Tomography System - User's Manual, Industrial Tomography Systems," 7.0, ITS System 2000 Version, April 2011. [Online].